Letter

Exciton spin Hall effect in arc-shaped strained WSe_2

A. Shubnic,[1,2] V. Shahnazaryan,[1,2,*] I. A. Shelykh,[3,4] and H. Rostami[5,†]

[1]*Abrikosov Center for Theoretical Physics, MIPT, Dolgoprudnyi, Moscow Region 141701, Russia*

[2]*Department of Physics, ITMO University, Saint Petersburg 197101, Russia*

[3]*Science Institute, University of Iceland, Dunhagi 3, IS-107, Reykjavik, Iceland*

[4]*Russian Quantum Center, Skolkovo IC, Bolshoy Bulvar 30 bld. 1, Moscow 121205, Russia*

[5]*Nordita, KTH Royal Institute of Technology and Stockholm University, Hannes Alfvéns väg 12, 10691 Stockholm, Sweden*

(Received 13 November 2023; revised 6 May 2024; accepted 10 May 2024; published 24 May 2024)

Generating a pure spin current using electrons, which have degrees of freedom beyond spin, such as electric charge and valley index, presents challenges. In response, we propose a mechanism based on intervalley exciton dynamics in *arc-shaped* strained transition metal dichalcogenides (TMDs) to achieve the *exciton spin Hall effect* in an electrically insulating regime, without the need for an external electric field. The interplay between strain gradients and strain-induced pseudomagnetic fields results in a net Lorentz force on long-lived intervalley excitons in WSe_2, carrying nonzero spin angular momentum. This process generates an exciton-mediated pure spin Hall current, resulting in opposite-sign spin accumulations and local magnetization on the two sides of the single-layer arc-shaped TMD. We demonstrate that the magnetic field induced by spin accumulation, at approximately ∼mT, can be detected using techniques such as superconducting quantum interference magnetometry or spatially resolved magneto-optical Faraday and Kerr rotations.

DOI: 10.1103/PhysRevB.109.L201409

Introduction. The spin Hall effect (SHE) was first introduced by D'yakonov, Perel' in 1971 [1], revisited by Hirsch in 1999 [2] and experimentally demonstrated in 2004 [3,4]. One of the versions of SHE, namely the intrinsic SHE arises from strong spin-orbit coupling resulting in the band structure quantum geometry (Berry curvature), and leading to the appearance of a transverse spin current when an electric field is applied, without the need of an external magnetic field. This effect generates edge spin accumulation, observed in GaAs-based semiconductors using magneto-optical Kerr rotation measurement [3]. The quantum spin Hall effect predicted in graphene [5] and two-dimensional (2D) electron gases [6] was experimentally verified in HgTe, revealing quantized spin-Hall conductance and absent charge-Hall conductance [7].

Among various 2D materials, monolayers of transition metal dichalcogenides (TMDs) [8] are of special interest. This is because of their remarkable compatibility with various semiconductor/dielectric platforms and their remarkable properties, such as peculiar 2D screening leading to dramatic modification of the interaction potential between the charged

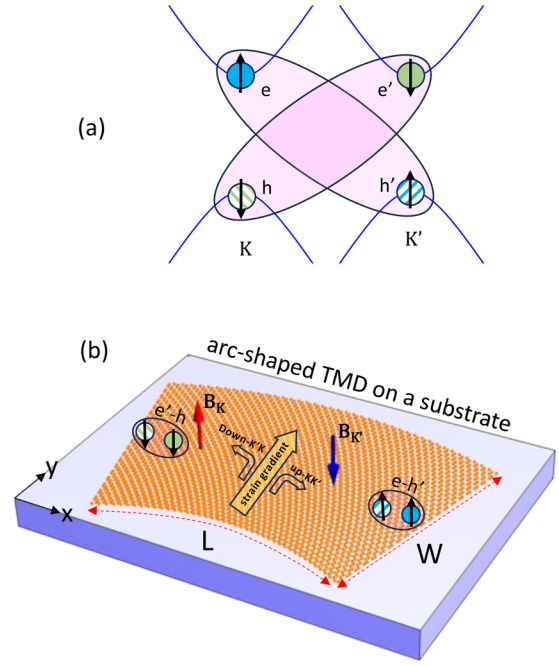

FIG. 1. (a) The scheme of the low-energy band structure with two intervalley dark excitonic states in WSe_2 monolayer. (b) The geometry of the proposed arc-shaped device designed to induce the exciton-mediated spin Hall effect in WSe_2. Introduction of a nonuniform strain gives rise to a pseudomagnetic field, generating the Lorentz forces leading to opposite transverse center-of-mass movement of up-KK′ and down-K′K-excitons. The maximum strain in the system is given by $W/2R$, where W and R represent the width and radius of the arc, respectively. The x direction corresponds to a zigzag crystallographic orientation.

*vanikshahnazaryan@gmail.com

†Present address: Department of Physics, University of Bath, Claverton Down, Bath BA2 7AY, United Kingdom; hr745@bath.ac.uk

carriers [9] and nontrivial spin and valley dynamics [10–13]. In particular, spin-valley coupling [14] in doped TMDs is anticipated to induce spin and valley Hall effects, whether arising from gating potentials or photoexcited density. However, since the trivial band gap is much larger than the spin-orbit coupling, MoS_2 and WSe_2 do not support quantum spin Hall effect in the insulating regime. Unlike 2H-TMDs, the 1T′ structure [15] of TMD materials is of greater topological interest as it supports the quantum spin Hall effect, even at relatively high temperatures such as 100 K in 1T′-WTe_2 [16–18].

Besides intriguing single electron properties, TMD monolayers possess a remarkable excitonic response as well. Direct energy band gap and relatively large reduced mass of an electron-hole pair combined with truly 2D nature of interacting electrons and holes results in extremely large excitonic binding energies (∼300 meV) which make TMD excitons stable even at room temperatures [19–21].

It should be noted, that the spin-orbit coupling in WSe_2 differs from that in MoS_2, which results in a reversed order of spin-polarized bands within the conduction band, so that the energy of dark intravalley spin-singlet excitons is below the energy of bright excitons [9]. Moreover, dark intervalley excitons formed in WSe_2 exhibit even stronger binding stability (it lies 16 meV below the spin-forbidden dark exciton state in WSe_2) and even longer lifetime since corresponding recombination process requires an intervalley transition mediated by a valley phonon [22]. The intervalley excitons bear a $(+1)$ spin for electron-hole pairs originating from the K-valley electron (e) and the K′-valley hole (h′) (denoted as *up*-KK′-*exciton* in the further discussion), and (-1) spin for electron-hole pairs arising from the K′-valley electron (e′) and the K-valley hole (h) (denoted as *down*-K′K-*exciton* in the further discussion). The high stability, long lifetime, electrical neutrality, and finite spin angular momentum of intervalley excitons in WSe_2 make them optimal candidates to mediate the pure spin Hall effect in 2D.

Being electrically neutral particles, excitons do not reveal any significant response to external electric and magnetic fields. However, one can use strain effects instead. 2D materials including graphene and TMD monolayers possess very rich strain physics primarily due to the sharing three-fold symmetry point groups. Static strain leads to the appearance of a pseudogauge field $\mathbf{A}$ [23] in addition to the conventional scalar deformation potential V. Because of the time-reversal symmetry, this pseudo-gauge field have different sign for electrons located at the valley points K and K′ which are time-reversal partners, $\mathbf{A}_{\mathrm{K}} = -\mathbf{A}_{\mathrm{K}'}$. An inhomogeneous strain leads to a non-uniform pseudogauge field that results in a pseudomagentic field $\mathbf{B}_{\mathrm{K}} = -\mathbf{B}_{\mathrm{K}'} = \nabla \times \mathbf{A}_{\mathrm{K}}$.

The case of a uniform pseudomagnetic field is particularly interesting as it allows the exploration of strain-induced cyclotron dynamics, Landau level formation and the quantum valley Hall effect [24]. Examples of experimental geometries generating such uniform pseudomagnetic fields, exceeding 100s of Tesla [25–27], include trigonal and hexagonal symmetric nanobubbles and arc-shaped straining [28–30]. The latter case, reported in a recent twisted bilayer graphene experiment [31], is particularly important, as it allows creation of a uniform pseudomagnetic fields across larger samples, which is not possible with nanobubbles.

In this study, we investigate the effects of the combination of strain-induced electric and magnetic fields on intervalley exciton transport in WSe_2, featuring an inverted spin-split conduction band. Our results reveal a distinctive pure spin Hall effect for intervalley excitons, which bear no electric or valley charge. We propose an arc-shaped WSe_2 setup depicted in Fig. 1(b) as a suitable geometry for the observation of the effect. In this situation, up-KK′-excitons and down-K′K-excitons will first drift along the y axis under a gradient of the scalar potential ∇V generated by strain, and gain a drift velocity $\mathbf{v}_d = -\mu_{\mathrm{X}} \nabla V$ with μ_{X} being the exciton mobility. These moving excitons are affected by the Lorentz force produced by strain-induced pseudomagnetic field and generating Hall-like transverse current. In the stationary regime, an electron-hole pair corresponding to a up-KK′-exciton feels the Lorentz force

$$\mathbf{f}_{\mathrm{up-KK'}} = \mathbf{v}_d \times (q_e \mathbf{B}_{\mathrm{K}} + q_{h'} \mathbf{B}_{\mathrm{K}'}) = 2e\mu_{\mathrm{X}} \nabla V \times \mathbf{B}, \tag{1}$$

where we took $q_e = -q_{h'} = -e$ and used that $\mathbf{B}_{\mathrm{K}} = -\mathbf{B}_{\mathrm{K}'} = \mathbf{B}$. The Lorentz force acting at a down-K′K-exciton has opposite direction, $\mathbf{f}_{\mathrm{down-K'K}} = -\mathbf{f}_{\mathrm{up-KK'}}$ and therefore up and down spins accumulate at opposite edges of the device as shown in Fig. 1(b).

While the dynamics of pseudomagnetoexcitons have been previously explored in strained graphene [32], here we present a robust argument supported by microscopic transport theory for the exciton-assisted spin Hall effect driven by nonuniform strain in single-layer TMD. Note, that the proposed mechanism is distinct from conventional exciton Hall effect in TMD monolayers, which is of valley-selective nature [33–37]. The Lorentz force acting on an intravalley exciton vanishes as both an electron and a hole feel the same pseudomagnetic field, and therefore the net force is zero. Note, however, that in this case pseudomagnetic field will result in the appearance of a dipole moment of a moving exciton, which leads to the appearance of the skew scattering term if an exciton interacts with an impurity and onset of the anomalous exciton Hall effect [38].

The quantitative model. In semiclassical picture, the dynamics of an intervalley exciton is described by the Newton's law (see Supplemental Material [39] for the detailed derivation):

$$\frac{\mathrm{d}\mathbf{p}}{\mathrm{d}t} = -\nabla V(\mathbf{r}) - 2e\xi \mathbf{v}_{\mathbf{p}} \times \mathbf{B}(\mathbf{r}), \tag{2}$$

where the index $\xi = +$ and $\xi = -$ denotes up-KK′-excitons and down-K′K-excitons, respectively, $\mathbf{v}_{\mathbf{p}} = \mathbf{p}/M$ is the particle velocity with M being the exciton mass. The transport properties of an ensemble of excitons are described by the Boltzmann equation for exciton distribution function $f_{\mathbf{p}}^{\xi}(\mathbf{r}, t)$ which reads

$$\begin{aligned} &\frac{\partial f_{\mathbf{p}}^{\xi}(\mathbf{r}, t)}{\partial t} + (-\nabla V(\mathbf{r}) - 2e\xi[\mathbf{v}_{\mathbf{p}} \times \mathbf{B}(\mathbf{r})]) \cdot \nabla_{\mathbf{p}} f_{\mathbf{p}}^{\xi}(\mathbf{r}, t) \\ &+ \mathbf{v}_{\mathbf{p}} \cdot \nabla f_{\mathbf{p}}^{\xi}(\mathbf{r}, t) = -\frac{f_{\mathbf{p}}^{\xi}(\mathbf{r}, t)}{\tau_{\mathrm{X}}} - \frac{f_{\mathbf{p}}^{\xi}(\mathbf{r}, t) - \bar{f}_{\mathbf{p}}^{\xi}(\mathbf{r}, t)}{\tau_{\mathrm{C}}} \\ &- \frac{f_{\mathbf{p}}^{\xi}(\mathbf{r}, t) - f_{\mathbf{p}}^{-\xi}(\mathbf{r}, t)}{2\tau_{\mathrm{S}}}. \end{aligned} \tag{3}$$

Note that $f_{\mathbf{p}}^{\xi}(\mathbf{r},t)$ is the local equilibrium density that follows Maxwell-Boltzmann distribution function. We used the relaxation time approximation, which accounts for exciton recombination with characteristic time τ_{X} and exciton scattering on phonons and impurities with characteristic time τ_{C}. The last term corresponds to exciton spin relaxation [40–44]. The exciton density is obtained by integrating the distribution function by momentum $\mathbf{p}$,

$$n^{\xi}(\mathbf{r},t)=\int\frac{\mathrm{d}^2\mathbf{p}}{(2\pi\hbar)^2}f_{\mathbf{p}}^{\xi}(\mathbf{r},t). \tag{4}$$

The dynamics of total exciton density $n=n^{+}+n^{-}$ and spin density $S_z=n^{+}-n^{-}$, related to spin polarization as $P_z=S_z/n$ are described by the following equations (see the derivation in [39], and the Ref. [45] therein):

$$\frac{\partial n(\mathbf{r},t)}{\partial t}+\boldsymbol{\nabla}\cdot\mathbf{j}(\mathbf{r},t)=-\frac{n(\mathbf{r},t)}{\tau_{\mathrm{X}}}, \tag{5}$$

$$\frac{\partial S_z(\mathbf{r},t)}{\partial t}+\boldsymbol{\nabla}\cdot\mathbf{j}^{\mathrm{S}}(\mathbf{r},t)=-\frac{S_z(\mathbf{r},t)}{\widetilde{\tau}_{\mathrm{X}}}, \tag{6}$$

where $1/\widetilde{\tau}_{\mathrm{X}}=1/\tau_{\mathrm{X}}+1/\tau_{\mathrm{S}}$ and the exciton number current density reads

$$\mathbf{j}(\mathbf{r},t)=\frac{\mathcal{J}\{n(\mathbf{r},t)\}}{1+[\tau\omega_{\mathrm{c}}(\mathbf{r})]^2}+\frac{\tau\omega_{\mathrm{c}}(\mathbf{r})}{1+[\tau\omega_{\mathrm{c}}(\mathbf{r})]^2}\hat{\mathbf{B}}\times\mathcal{J}\{S_z(\mathbf{r},t)\}, \tag{7}$$

and the exciton spin current density follows

$$\mathbf{j}^{\mathrm{S}}(\mathbf{r},t)=\frac{\mathcal{J}\{S_z(\mathbf{r},t)\}}{1+[\tau\omega_{\mathrm{c}}(\mathbf{r})]^2}+\frac{\tau\omega_{\mathrm{c}}(\mathbf{r})}{1+[\tau\omega_{\mathrm{c}}(\mathbf{r})]^2}\hat{\mathbf{B}}\times\mathcal{J}\{n(\mathbf{r},t)\}. \tag{8}$$

Here, $\omega_{\mathrm{c}}(\mathbf{r})=2eB(\mathbf{r})/M$ is the exciton cyclotron frequency, with B being the modulus of the strain-induced pseudomagnetic field, and $\hat{\mathbf{B}}=\mathbf{B}/B$. The drift-diffusion current functional in the presence of a strain gradient force, $\boldsymbol{\nabla}V$, is defined as

$$\mathcal{J}\{Y(\mathbf{r},t)\}=-D_{\mathrm{X}}\boldsymbol{\nabla}Y(\mathbf{r},t)-\mu_{\mathrm{X}}Y(\mathbf{r},t)\boldsymbol{\nabla}V(\mathbf{r}), \tag{9}$$

where $\mu_{\mathrm{X}}=\tau/M$ is the exciton mobility, with $\tau=[1/\tau_{\mathrm{C}}+1/\tau_{\mathrm{X}}+1/(2\tau_{\mathrm{S}})]^{-1}$ being an effective relaxation time. The diffusion constant is given by $D_{\mathrm{X}}=\mu_{\mathrm{X}}(k_{\mathrm{B}}T)$, where k_{B} is the Boltzmann constant and T is the temperature. It is worth to remind the reader that considered semiclassical formalism is valid when $\omega_{\mathrm{c}}\tau\ll 1$, yielding in $\{1+(\tau\omega_c)^2\}^{-1}\approx 1-(\tau\omega_c)^2$. In the opposite regime the system is driven into a quantum regime where Landau levels are formed and a full quantum description of magnetoexcitons is required [32,46].

In addition to the quantitative correction to the longitudinal drift-diffusion current components described by first terms of Eqs. (7) and (8), pseudomagnetic field generates transverse Hall current components for both number and spin channels, as described by the second terms in Eqs. (7) and (8).

We further consider the specific arc-shaped deformation that generates a uniform pseudomagentic field. Arc-shaped strain is defined by an in-plane displacement field $(u_x,u_y)=(xy/R,-x^2/2R)$, where (x,y) are measured from the ribbon center and R is the bending radius of the arc-shaped TMD flake. The scalar and gauge fields are given in terms of the strain tensor elements $u_{ij}=(\partial_i u_j+\partial_j u_i)/2$ as $V=V_0(u_{xx}+u_{yy})$ and $\mathbf{A}_{\mathrm{K}}=(\beta\phi_0/2\pi a_0)(u_{xx}-u_{yy},-2u_{xy})$ and read

$$\mathbf{A}_{\mathrm{K}}=\frac{\beta\phi_0}{2\pi a_0}\frac{y}{R}\hat{\mathbf{x}},\quad V=V_0\frac{y}{R}, \tag{10}$$

where unity vector $\hat{\mathbf{x}}$ indicates a zigzag orientation in the hexagonal lattice. The constant pseudomagnetic field with opposite signs in the two valleys, is thus given by

$$|\mathbf{B}|=\beta\phi_0/(2\pi a_0 R), \tag{11}$$

with a corresponding magnetic length of $\ell_B=\sqrt{2a_0R/\beta}$, where $\phi_0=h/2e$ is the magnetic flux quantum, $\beta\sim 3$ is the Grünisen parameter describing electron-phonon coupling [47,48], $a=a_0\sqrt{3}$ is the lattice constant. For the constant pseudomagnetic field $\omega_{\mathrm{c}}(\mathbf{r})=\omega_{\mathrm{c}}$ one has $\boldsymbol{\nabla}(\tau\omega_{\mathrm{c}}D_{\mathrm{X}}\boldsymbol{\nabla}n^{\xi}\times\hat{\mathbf{B}})=0$, so that the respective terms can be discarded in Eqs. (7) and (8).

Results and discussion. We simulate the macroscopic transport equations (5) with initial Gaussian distributions $n^{\xi}=n_0e^{-(x^2+y^2)/(2\Delta^2)}$, where Δ is the characteristic size of an initial excitonic packet. In our numerical calculations we set $\Delta=0.5$ μm, $R=5$ μm, $\tau_{\mathrm{C}}=0.26$ ps [49], $T=300$ K, $V_0=300$ meV [50], $\tau_{\mathrm{X}}=200$ ps [22], $M=0.75\ m_0$, with m_0 being the free electron mass [51]. The spin relaxation time is estimated as $\tau_{\mathrm{S}}=47$ ps [39]. The respective pseudomagnetic field is then $B\approx 2.15$ T.

The evolution of intervalley excitons' number and spin densities under the influence of strain-induced driving fields are presented in Fig. 2. As seen in Figs. 2(a) and 2(b), the total density n gradually broadens by diffusion, and the distribution maximum shifts in the y-direction due to strain-induced exciton drift. The cross-sections of the total exciton density at different time snapshots shown in Fig. 2(c) indicate the overall longitudinal drift in the y direction. The transverse separation of two species of intervalley excitons, characterized by exciton spin density S_z and polarization P_z, is depicted in Figs. 2(d) and 2(e), respectively. The cross sections of the spin density in Fig. 2(f) further confirm the spin Hall current in the x direction and the spin accumulation on two sides of the 2D materials are almost identical to the electronic spin Hall effect [3]. Lower temperatures enhance the transverse separation of exciton spin density S_z (Fig. S1 in Ref. [39]). This results from reduced diffusion and extended spin relaxation time at low temperatures, enhancing the Hall drift.

In order to quantify the average strength of exciton spin Hall effect relative to average longitudinal exciton number current, we introduce a Hall angle θ. For a uniform pseudomagnetic field it reads

$$\tan\theta=\frac{\langle \mathrm{j}_x^{\mathrm{S}}\rangle}{\langle \mathrm{j}_y\rangle}=\frac{\int \mathrm{j}_x^{\mathrm{S}}\mathrm{d}x\mathrm{d}y}{\int \mathrm{j}_y\mathrm{d}x\mathrm{d}y}=-\tau\omega_{\mathrm{c}}=-\frac{2eB\tau}{M}, \tag{12}$$

With $\tan\theta=\langle \mathrm{j}_x^{\mathrm{S}}\rangle/\langle \mathrm{j}_y\rangle\propto\tau\approx\tau_{\mathrm{C}}$, where $\tau_{\mathrm{C}}\ll\tau_{\mathrm{S}}<\tau_{\mathrm{X}}$ [39], the Hall angle $\tan\theta$ and spin polarization S_z exhibit nearly linear growth with τ_{C}. The spatial distribution of S_z across different τ_{C} values is depicted in Fig. S2 [39], highlighting the observable effect under varying levels of disorder and imperfection parameterized by τ_{C}. The increase in τ_{C} leads to a reduced spin relaxation rate, $\tau_{\mathrm{S}}\propto 1/\tau_{\mathrm{C}}$, following the D'yakonov-Perel' spin-relaxation mechanism [40–44,52,53],

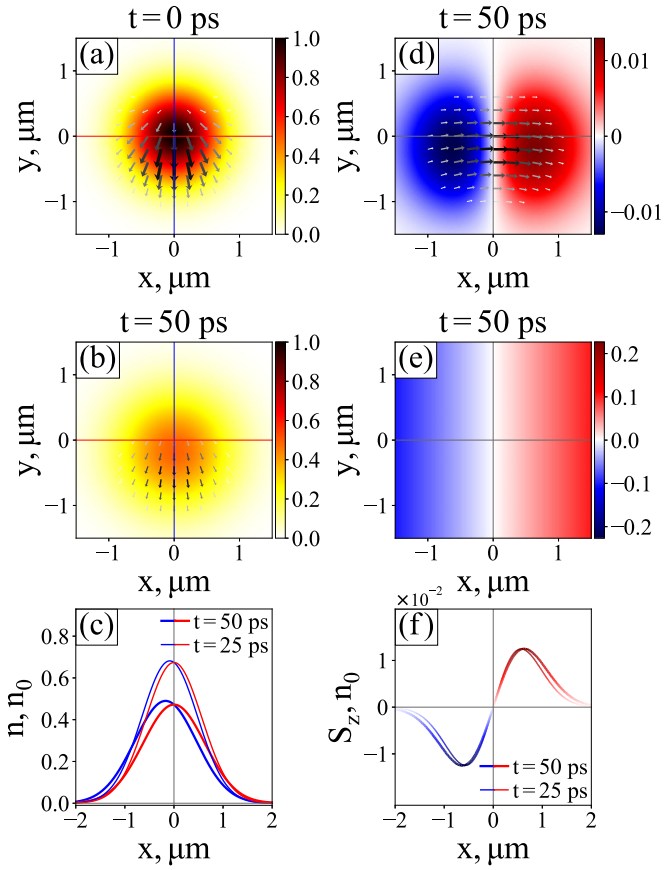

FIG. 2. Strain-induced evolution of intervalley excitons' number and spin densities. (a) and (b) depict snapshots of the total exciton density, denoted as n (in units of n_0). These snapshots are taken for a system with a radius of $R = 5$ μm and a temperature of $T = 300$ K at two time points: $t = 0$ and $t = 50$ ps, respectively. The vector field arrows indicate the exciton current density, denoted as $\mathbf{j}$. (c) Cross sections of the total exciton density n along the x axis (depicted by the red curve) and the y axis (depicted by the blue curve). The temporal evolution results in the broadening of the Gaussian exciton packet and its drift along the y axis, attributed to the strain gradient ∇V. (d) and (e) show snapshots of the exciton spin density S_z (in units of n_0) and the spin polarization $P_z = S_z/n$ at $t = 50$ ps, respectively. The vector field arrows in (d) illustrate the respective current density $\mathbf{j}^S$. A valley-dependent pseudomagnetic field leads to the separation of intervalley excitons with opposite spins along the x axis. (f) Cross section of the exciton spin density S_z along the x axis. In (c) and (f), the thin curves correspond to $t = 25$ ps, and the thick curves represent $t = 50$ ps.

resulting in a saturating dependence of S_z on τ_C (Fig. S2(d) in Ref. [39]).

Furthermore, as seen in Eq. (12), the Hall angle scales with the arc radius as $\tan\theta \propto B \propto 1/R$ and it can be enhanced by reducing the arc radius that implies increasing the curvature. Recently, arc-shaped deformation was experimentally achieved in graphene using a nanomanipulator and an atomic force microscope tip [31]. Given a local deflection $d(x)$ along the y direction in a ribbon oriented along the x direction, the *local* curvature radius is determined by $R(x) = |(1 + [\partial_x d(x)]^2)^{3/2}/\partial_x^2 d(x)|$. The strain $\varepsilon(x, y) = y/R(x)$, governing both scalar and vector potentials (Eq. (10)), reaches its maximum, $\varepsilon_{\max} = \pm W/2R$, at the ribbon edges $y = \pm W/2$. For instance, with a ribbon width $W = 1\mu$ and $R = 10\mu$, this yields $\varepsilon_{\max} \approx 5\%$. The dependence of S_z on the arc radius R is illustrated in Fig. S3 in Ref. [39]. Single-layer WSe_2 exhibits robust mechanical properties [54–57] with a reasonably large Young's Modulus (∼250 GPa [58]), bending rigidity (∼12 eV [59]), a maximum strain tolerance of ∼7.3% in multilayer systems [60], and a predicted value ∼19.7% in single-layer WSe_2 [58], securing thus the robustness for strain engineering and stability against out-of-plane buckling under arc-shaped deformations.

Experimental realization. An intervalley exciton is the lowest energy exciton state, lying 16 meV below the spin-forbidden dark exciton state in WSe_2 [22]. The respective peak is clearly visible in photoluminescence spectrum at low free carrier concentration and under nonresonant optical excitation. The optical excitation/recombination of an intervalley exciton is accompanied by the respective absorption/emission of a chiral phonon [61], mediating the electron intervalley transition. In this process, the polarization of the absorbed/emitted photon is determined by the spin orientation of a hole, for which spin-valley locking holds. As intervalley excitons have sufficiently large lifetime of about 200 ps, in the considered configuration of arc-shaped WSe_2 monolayer after sufficiently long time away from the initial localized excitation pump spot the luminescence will have opposite circular polarizations, corresponding to the opposite spins of the excitons for positive and negative values of x coordinate. This can be probed experimentally by near field measurement.

Moreover, spatial separation of spin polarizations generates an effective magnetic field. Indeed, the quantity $S_z(x, y) = n^+(x, y) - n^-(x, y)$ is associated with the spin angular momentum density. Taking into account the intervalley exciton g factor $g \approx -12$ [22], one can derive the magnetic moment density in a 2D system as $m(x, y) = g\mu_B S_z(x, y)$ where $\mu_B = 57.9 \times 10^{-6}$ eV/T is the Bohr magneton [62]. Accounting for finite thickness of our 2D material, $d \approx 0.7$ nm, we introduce an effective 3D magnetization,

$$\mathcal{M}(x, y) = \frac{g\mu_B}{d} n(x, y) P_z(x, y) \approx \frac{g\mu_B}{d} n_0 P_z(x, y), \qquad (13)$$

which allows us to estimate the corresponding magnetic field $B_0 = \mu_0 \mathcal{M}$ where μ_0 is the magnetic permeability of the vacuum. For realistic exciton concentrations $n_0 \sim 10^{12}$ cm^{-2} this gives an estimated value of $B_0 \sim 0.002$ T, which is quite significant and falls within the range of magnetic fields typically measured in the spin Hall effect in 2D electron gas systems [3].

The exciton spin Hall effect results in a local magnetization (and magnetic field) of sufficient magnitude to be probed by magneto-optical techniques like Faraday and Kerr rotation spectroscopy. The linear polarization rotation angle can be calculated using

$$\varphi_F = \mathcal{V} d B_0. \qquad (14)$$

The Verdet constant in TMD monolayers is shown to be strongly frequency dependent and it can be as large as $\mathcal{V}d \sim 5 \times 10^{-6}$ rad/T [63,64], which yields $\varphi_F \sim 10^{-8}$ rad. Rotation angle can be further amplified by placing a monolayer

in an optical cavity [65,66]. Furthermore, we can enhance the effect by increasing the level of straining. The maximum strain in an arc-shaped geometry occurs at the outer edges, where the maximum strain is given by $\varepsilon_{\max} = \pm W/2R$, as shown in Fig. 1. When considering a fixed maximum strain, we can achieve an enhanced pseudomagnetic field by using smaller arc radii in nanoribbon systems with a narrow width W. In addition, we can utilize nanobubble structures made of WS_2 and WSe_2, which can generate substantial pseudomagnetic fields in the range of hundreds of Tesla [25–27], thereby leading to a significantly large spin accumulation due to the strain-induced exciton spin Hall effect.

Conclusion. We proposed a mechanism of spin Hall effect for intervalley excitons in arc-shaped monolayers of WSe_2. In the considered geometry, the strain gradient results in both the drifting force and valley-dependent net Lorentz force acting on intervalley excitons, resulting in the onset of the transverse spin current. The proposed effect can be directly probed via spatially resolved near field photoluminescence spectroscopy, and pump-probe Faraday or Kerr rotation techniques. This effect is quite general and can also manifest itself in other indirect excitonic systems with hexagonal symmetry, such as bilayer and bulk TMD systems, where electrons and holes belong to different valley points that are time-reversal counterparts of each other. Exploring the impact of sound-induced pseudogauge fields, such as the acoustogalvanic effect [67,68]—recently observed in graphene [69]—on exciton spin transport, opens the possibility of extending this effect to acoustospin modulation effects.

Acknowledgments. The research is supported by the Ministry of Science and Higher Education of the Russian Federation (Goszadaniye) Project No. FSMG-2023-0011. The derivation of theoretical model was funded by Russian Science Foundation, Project No. 21-72-10100. The reported study was funded by RFBR and SC RA, Project No. 20-52-05005. V.S. acknowledges the support of 'Basis' Foundation (Project No. 22-1-3-43-1). H.R. acknowledges the support of Swedish Research Council (VR Starting Grant No. 2018-04252).

[1] M. I. Dyakonov and V. I. Perel, Current-induced spin orientation of electrons in semiconductors, Phys. Lett. A **35**, 459 (1971).
[2] J. E. Hirsch, Spin Hall effect, Phys. Rev. Lett. **83**, 1834 (1999).
[3] Y. K. Kato, R. C. Myers, A. C. Gossard, and D. D. Awschalom, Observation of the spin Hall effect in semiconductors, Science **306**, 1910 (2004).
[4] J. Wunderlich, B. Kaestner, J. Sinova, and T. Jungwirth, Experimental observation of the spin-Hall effect in a two-dimensional spin-orbit coupled semiconductor system, Phys. Rev. Lett. **94**, 047204 (2005).
[5] C. L. Kane and E. J. Mele, Quantum spin Hall effect in graphene, Phys. Rev. Lett. **95**, 226801 (2005).
[6] B. A. Bernevig and S.-C. Zhang, Quantum spin Hall effect, Phys. Rev. Lett. **96**, 106802 (2006).
[7] B. A. Bernevig, T. L. Hughes, and S.-C. Zhang, Quantum spin Hall effect and topological phase transition in HgTe quantum wells, Science **314**, 1757 (2006).
[8] K. F. Mak, C. Lee, J. Hone, J. Shan, and T. F. Heinz, Atomically thin MoS_2: A new direct-gap semiconductor, Phys. Rev. Lett. **105**, 136805 (2010).
[9] G. Wang, A. Chernikov, M. M. Glazov, T. F. Heinz, X. Marie, T. Amand, and B. Urbaszek, Colloquium: Excitons in atomically thin transition metal dichalcogenides, Rev. Mod. Phys. **90**, 021001 (2018).
[10] W. Yao, D. Xiao, and Q. Niu, Valley-dependent optoelectronics from inversion symmetry breaking, Phys. Rev. B **77**, 235406 (2008).
[11] P. Dey, L. Yang, C. Robert, G. Wang, B. Urbaszek, X. Marie, and S. A. Crooker, Gate-controlled spin-valley locking of resident carriers in WSe_2 monolayers, Phys. Rev. Lett. **119**, 137401 (2017).
[12] X.-X. Zhang, Y. Lai, E. Dohner, S. Moon, T. Taniguchi, K. Watanabe, D. Smirnov, and T. F. Heinz, Zeeman-induced valley-sensitive photocurrent in monolayer MoS_2, Phys. Rev. Lett. **122**, 127401 (2019).
[13] A. Avsar, H. Ochoa, F. Guinea, B. Özyilmaz, B. J. van Wees, and I. J. Vera-Marun, Colloquium: Spintronics in graphene and other two-dimensional materials, Rev. Mod. Phys. **92**, 021003 (2020).
[14] D. Xiao, G.-B. Liu, W. Feng, X. Xu, and W. Yao, Coupled spin and valley physics in monolayers of MoS_2 and other group-vi dichalcogenides, Phys. Rev. Lett. **108**, 196802 (2012).
[15] X. Qian, J. Liu, L. Fu, and J. Li, Quantum spin Hall effect in two-dimensional transition metal dichalcogenides, Science **346**, 1344 (2014).
[16] S. Wu, V. Fatemi, Q. D. Gibson, K. Watanabe, T. Taniguchi, R. J. Cava, and P. Jarillo-Herrero, Observation of the quantum spin Hall effect up to 100 kelvin in a monolayer crystal, Science **359**, 76 (2018).
[17] Y. Shi, J. Kahn, B. Niu, Z. Fei, B. Sun, X. Cai, B. A. Francisco, D. Wu, Z.-X. Shen, X. Xu, D. H. Cobden, and Y.-T. Cui, Imaging quantum spin Hall edges in monolayer WTe_2, Sci. Adv. **5**, eaat8799 (2019).
[18] J. H. Garcia, M. Vila, C.-H. Hsu, X. Waintal, V. M. Pereira, and S. Roche, Canted persistent spin texture and quantum spin Hall effect in WTe_2, Phys. Rev. Lett. **125**, 256603 (2020).
[19] K. F. Mak, K. He, C. Lee, G. H. Lee, J. Hone, T. F. Heinz, and J. Shan, Tightly bound trions in monolayer MoS_2, Nat. Mater. **12**, 207 (2013).
[20] J. S. Ross, S. Wu, H. Yu, N. J. Ghimire, A. M. Jones, G. Aivazian, J. Yan, D. G. Mandrus, D. Xiao, W. Yao, and X. Xu, Electrical control of neutral and charged excitons in a monolayer semiconductor, Nat. Commun. **4**, 1474 (2013).
[21] M. M. Ugeda, A. J. Bradley, S.-F. Shi, F. H. da Jornada, Y. Zhang, D. Y. Qiu, W. Ruan, S.-K. Mo, Z. Hussain, Z.-X. Shen, F. Wang, S. G. Louie, and M. F. Crommie, Giant bandgap renormalization and excitonic effects in a monolayer transition metal dichalcogenide semiconductor, Nat. Mater. **13**, 1091 (2014).
[22] Z. Li, T. Wang, C. Jin, Z. Lu, Z. Lian, Y. Meng, M. Blei, M. Gao, T. Taniguchi, K. Watanabe *et al.*, Momentum-dark intervalley

exciton in monolayer tungsten diselenide brightened via chiral phonon, ACS Nano **13**, 14107 (2019).
[23] M. A. H. Vozmediano, M. I. Katsnelson, and F. Guinea, Gauge fields in graphene, Phys. Rep. **496**, 109 (2010).
[24] F. Guinea, M. I. Katsnelson, and A. K. Geim, Energy gaps and a zero-field quantum Hall effect in graphene by strain engineering, Nat. Phys. **6**, 30 (2010).
[25] N. Levy, S. A. Burke, K. L. Meaker, M. Panlasigui, A. Zettl, F. Guinea, A. H. C. Neto, and M. F. Crommie, Strain-induced pseudomagnetic fields greater than 300 tesla in graphene nanobubbles, Science **329**, 544 (2010).
[26] A. Georgi, P. Nemes-Incze, R. Carrillo-Bastos, D. Faria, S. Viola Kusminskiy, D. Zhai, M. Schneider, D. Subramaniam, T. Mashoff, N. M. Freitag, M. Liebmann, M. Pratzer, L. Wirtz, C. R. Woods, R. V. Gorbachev, Y. Cao, K. S. Novoselov, N. Sandler, and M. Morgenstern, Tuning the pseudospin polarization of graphene by a pseudomagnetic field, Nano Lett. **17**, 2240 (2017).
[27] P. Nigge, A. C. Qu, É. Lantagne-Hurtubise, E. Mårsell, S. Link, G. Tom, M. Zonno, M. Michiardi, M. Schneider, S. Zhdanovich, G. Levy, U. Starke, C. Gutiérrez, D. Bonn, S. A. Burke, M. Franz, and A. Damascelli, Room temperature strain-induced Landau levels in graphene on a wafer-scale platform, Sci. Adv. **5**, eaaw5593 (2019).
[28] T. Low and F. Guinea, Strain-induced pseudomagnetic field for novel graphene electronics, Nano Lett. **10**, 3551 (2010).
[29] H. Rostami and R. Asgari, Electronic structure and layer-resolved transmission of bilayer graphene nanoribbon in the presence of vertical fields, Phys. Rev. B **88**, 035404 (2013).
[30] H. Rostami, R. Roldán, E. Cappelluti, R. Asgari, and F. Guinea, Theory of strain in single-layer transition metal dichalcogenides, Phys. Rev. B **92**, 195402 (2015).
[31] M. Kapfer, B. S. Jessen, M. E. Eisele, M. Fu, D. R. Danielsen, T. P. Darlington, S. L. Moore, N. R. Finney, A. Marchese, V. Hsieh, P. Majchrzak, Z. Jiang, D. Biswas, P. Dudin, J. Avila, K. Watanabe, T. Taniguchi, S. Ulstrup, P. Bøggild, P. J. Schuck, D. N. Basov, J. Hone, and C. R. Dean, Programming twist angle and strain profiles in 2D materials, Science **381**, 677 (2023).
[32] O. L. Berman, R. Y. Kezerashvili, Y. E. Lozovik, and K. G. Ziegler, Strain-induced quantum Hall phenomena of excitons in graphene, Sci. Rep. **12**, 2950 (2022).
[33] M. Onga, Y. Zhang, T. Ideue, and Y. Iwasa, Exciton Hall effect in monolayer MoS_2, Nat. Mater. **16**, 1193 (2017).
[34] Y.-M. Li, J. Li, L.-K. Shi, D. Zhang, W. Yang, and K. Chang, Light-induced exciton spin Hall effect in van der Waals heterostructures, Phys. Rev. Lett. **115**, 166804 (2015).
[35] T. Yu and M. W. Wu, Valley depolarization dynamics and valley Hall effect of excitons in monolayer and bilayer MoS_2, Phys. Rev. B **93**, 045414 (2016).
[36] Z. Huang, Y. Liu, K. Dini, Q. Tan, Z. Liu, H. Fang, J. Liu, T. Liew, and W. Gao, Robust room temperature valley Hall effect of interlayer excitons, Nano Lett. **20**, 1345 (2020).
[37] M. M. Glazov and L. E. Golub, Skew scattering and side jump drive exciton valley Hall effect in two-dimensional crystals, Phys. Rev. Lett. **125**, 157403 (2020).
[38] V. K. Kozin, V. A. Shabashov, A. V. Kavokin, and I. A. Shelykh, Anomalous exciton Hall effect, Phys. Rev. Lett. **126**, 036801 (2021).
[39] See Supplemental Material at http://link.aps.org/supplemental/10.1103/PhysRevB.109.L201409 for the derivation Lorentz force acting on exciton center-of-mass dynamics, and the derivation of macropsopic transport equations,
[40] M. Z. Maialle, E. A. de Andradae Silva, and L. J. Sham, Exciton spin dynamics in quantum wells, Phys. Rev. B **47**, 15776 (1993).
[41] M. M. Glazov, T. Amand, X. Marie, D. Lagarde, L. Bouet, and B. Urbaszek, Exciton fine structure and spin decoherence in monolayers of transition metal dichalcogenides, Phys. Rev. B **89**, 201302(R) (2014).
[42] C. R. Zhu, K. Zhang, M. Glazov, B. Urbaszek, T. Amand, Z. W. Ji, B. L. Liu, and X. Marie, Exciton valley dynamics probed by Kerr rotation in WSe_2 monolayers, Phys. Rev. B **90**, 161302(R) (2014).
[43] X. Jiang, Q. Zheng, Z. Lan, W. A. Saidi, X. Ren, and J. Zhao, Real-time *GW*-BSE investigations on spin-valley exciton dynamics in monolayer transition metal dichalcogenide, Sci. Adv. **7**, eabf3759 (2021).
[44] Z. An, P. Soubelet, Y. Zhumagulov, M. Zopf, A. Delhomme, C. Qian, P. E. Faria Junior, J. Fabian, X. Cao, J. Yang, A. V. Stier, F. Ding, and J. J. Finley, Strain control of exciton and trion spin-valley dynamics in monolayer transition metal dichalcogenides, Phys. Rev. B **108**, L041404 (2023).
[45] A. Jüngel, *Transport Equations for Semiconductors*, Vol. 773 (Springer, Berlin, 2009).
[46] V. E. Bisti, A. B. Van'kov, A. S. Zhuravlev, and L. V. Kulik, Magnetoexcitons in two-dimensional electronic systems, Phys. Usp. **58**, 315 (2015).
[47] H. Rostami, F. Guinea, M. Polini, and R. Roldán, Piezoelectricity and valley Chern number in inhomogeneous hexagonal 2D crystals, npj 2D Materials and Applications **2**, 15 (2018).
[48] V. Shahnazaryan and H. Rostami, Nonlinear exciton drift in piezoelectric two-dimensional materials, Phys. Rev. B **104**, 085405 (2021).
[49] F. Cadiz, C. Robert, E. Courtade, M. Manca, L. Martinelli, T. Taniguchi, K. Watanabe, T. Amand, A. Rowe, D. Paget *et al.*, Exciton diffusion in WSe_2 monolayers embedded in a van der waals heterostructure, Appl. Phys. Lett. **112**, 152106 (2018).
[50] H. Moon, G. Grosso, C. Chakraborty, C. Peng, T. Taniguchi, K. Watanabe, and D. Englund, Dynamic exciton funneling by local strain control in a monolayer semiconductor, Nano Lett. **20**, 6791 (2020).
[51] A. Kormányos, G. Burkard, M. Gmitra, J. Fabian, V. Zólyomi, N. D. Drummond, and V. Fal'ko, **k.p** theory for two-dimensional transition metal dichalcogenide semiconductors, 2D Mater. **2**, 022001 (2015).
[52] P. Boross, B. Dóra, A. Kiss, and F. Simon, A unified theory of spin-relaxation due to spin-orbit coupling in metals and semiconductors, Sci. Rep. **3**, 3233 (2013).
[53] M. W. Wu, J. H. Jiang, and M. Q. Weng, Spin dynamics in semiconductors, Phys. Rep. **493**, 61 (2010).
[54] W. Ding, D. Han, J. Zhang, and X. Wang, Mechanical responses of WSe_2 monolayers: a molecular dynamics study, Mater. Res. Express **6**, 085071 (2019).
[55] A. Castellanos-Gomez, M. Poot, G. A. Steele, H. S. J. van der Zant, N. Agraït, and G. Rubio-Bollinger, Elastic properties of freely suspended MoS_2 nanosheets, Adv. Mater. **24**, 772 (2012).
[56] H. Jiang, L. Zheng, Z. Liu, and X. Wang, Two-dimensional materials: From mechanical properties to flexible mechanical sensors, InfoMat **2**, 1077 (2020).

[57] C. Androulidakis, K. Zhang, M. Robertson, and S. Tawfick, Tailoring the mechanical properties of 2D materials and heterostructures, 2D Mater. **5**, 032005 (2018).

[58] A. Falin, M. Holwill, H. Lv, W. Gan, J. Cheng, R. Zhang, D. Qian, M. R. Barnett, E. J. G. Santos, K. S. Novoselov, T. Tao, X. Wu, and L. H. Li, Mechanical properties of atomically thin tungsten dichalcogenides: Ws_2, WSe_2, and WTe_2, ACS Nano **15**, 2600 (2021).

[59] J. Zhao, Q. Deng, T. H. Ly, G. H. Han, G. Sandeep, and M. H. Rümmeli, Two-dimensional membrane as elastic shell with proof on the folds revealed by three-dimensional atomic mapping, Nat. Commun. **6**, 8935 (2015).

[60] R. Zhang, V. Koutsos, and R. Cheung, Elastic properties of suspended multilayer WSe_2, Appl. Phys. Lett. **108**, 042104 (2016).

[61] H. Zhu, J. Yi, M.-Y. Li, J. Xiao, L. Zhang, C.-W. Yang, R. A. Kaindl, L.-J. Li, Y. Wang, and X. Zhang, Observation of chiral phonons, Science **359**, 579 (2018).

[62] E. Liu, J. van Baren, T. Taniguchi, K. Watanabe, Y.-C. Chang, and C. H. Lui, Magnetophotoluminescence of exciton Rydberg states in monolayer WSe_2, Phys. Rev. B **99**, 205420 (2019).

[63] J. Have, N. M. R. Peres, and T. G. Pedersen, Excitonic magneto-optics in monolayer transition metal dichalcogenides: From nanoribbons to two-dimensional response, Phys. Rev. B **100**, 045411 (2019).

[64] A. Ferreira, J. Viana-Gomes, Y. V. Bludov, V. Pereira, N. M. R. Peres, and A. H. Castro Neto, Faraday effect in graphene enclosed in an optical cavity and the equation of motion method for the study of magneto-optical transport in solids, Phys. Rev. B **84**, 235410 (2011).

[65] A. V. Kavokin, M. R. Vladimirova, M. A. Kaliteevski, O. Lyngnes, J. D. Berger, H. M. Gibbs, and G. Khitrova, Resonant Faraday rotation in a semiconductor microcavity, Phys. Rev. B **56**, 1087 (1997).

[66] H. Da, L. Gao, Y. An, H. Zhang, and X. Yan, Cavity-induced enhancement of magneto-optic effects in monolayer transition metal dichalcogenides, Adv. Opt. Mater. **6**, 1701175 (2018).

[67] P. O. Sukhachov and H. Rostami, Acoustogalvanic effect in Dirac and Weyl semimetals, Phys. Rev. Lett. **124**, 126602 (2020).

[68] P. Bhalla, G. Vignale, and H. Rostami, Pseudogauge field driven acoustoelectric current in two-dimensional hexagonal dirac materials, Phys. Rev. B **105**, 125407 (2022).

[69] P. Zhao, C. H. Sharma, R. Liang, C. Glasenapp, L. Mourokh, V. M. Kovalev, P. Huber, M. Prada, L. Tiemann, and R. H. Blick, Acoustically induced giant synthetic Hall voltages in graphene, Phys. Rev. Lett. **128**, 256601 (2022).